RSC Sustainability

ROYAL SOCIETY OF CHEMISTRY

COMMUNICATION

View Article Online
View Journal

Cite this: DOI: 10.1039/d5su00707k

Received 26th August 2025
Accepted 9th December 2025

DOI: 10.1039/d5su00707k

rsc.li/rscsus

Sustainable remanufacturing of mesoscopic carbon perovskite solar cells using green solvents

Karen Valadez-Villalobos, [a] Carys Worsley, [a] Rodrigo Garcia-Rodriguez,[a] Trystan Watson [a] and Matthew Davies [ab]

We present a green-solvent remanufacturing strategy for mesoscopic carbon-based perovskite solar cells (CPSCs) that enables complete recovery of the printed device stack. By immersing aged devices in γ-valerolactone (GVL), the perovskite absorber can be selectively removed without harming the underlying mesoporous carbon scaffold. Fresh perovskite is then reinfiltrated, restoring up to 89% of the device's first life power conversion efficiency (PCE). This sustainable method offers a promising route toward circularity in scalable perovskite photovoltaic technologies.

The large-scale deployment of photovoltaic (PV) technologies is central to global strategies for energy decarbonisation and achieving net-zero targets. This involves a projected global cumulative PV capacity of approximately 4500 GW by 2050,[1] an unprecedented scale which introduces several critical challenges concerning an adequate end-of-life (EOL) management and recovery of critical materials.[2,3] With the accelerated deployment of silicon PV, it is projected that recycling or repurposing end-of-life panels could unlock around 78 million tonnes of raw materials and valuable components by 2050, with an estimated value of USD 15 billion if reintegrated into the economy.[4] However, present module designs and the lack of adequate infrastructure for recycling and remanufacturing remain major barriers to effective material recovery.[5] These limitations not only restrict access to critical raw materials locked within solar panels, but also lead to the loss of the substantial embedded energy and carbon footprint associated with initial module fabrication, impacts that are reproduced with each new production cycle.[6,7]

Emerging PV technologies present a unique opportunity to embed circularity principles at the design stage, enabling efficient remanufacturing and optimised end-of-life management while minimising material loss and environmental impact.[8,9]

Sustainability spotlight

Circular design, the use of less toxic materials and processes, and reliance on abundant, low-cost resources are critical to ensuring photovoltaic technologies fulfil their role in the energy transition while remaining sustainable over the long term. To avoid the lock-in of valuable resources, a challenge already faced with decommissioned panels, emerging technologies must incorporate these considerations from the design stage. We present a remanufacturing pathway for carbon-based mesoscopic perovskite solar cells, a scalable and inexpensive architecture, enabling reuse of the full stack with reduced material and energy demand. By extending device lifetimes and lowering environmental impact, this work illustrates how emerging photovoltaic technologies can support a circular energy economy and advance SDGs 7 (Clean Energy), 12 (Responsible Production), and 13 (Climate Action).

Among emerging PV technologies, perovskite solar cells (PSCs) show exceptional promise due to their high-power conversion efficiencies, reaching up to 27% in single-junction devices,[10] and their advantageous solution-based, low-temperature fabrication processes.

Research into material recovery and recycling strategies for perovskite solar cells (PSCs) has recently accelerated, with most efforts focused on conventional n–i–p device architectures.[11–15] While these conventional configurations deliver excellent performance, their scalability is limited by the use of expensive materials, such as spiro-OMeTAD and noble metals like gold or silver, as well as fabrication methods that are difficult to scale up, including spin coating and metal evaporation. Moreover, most recovery methods reported to date rely on dissolving the device layers, which results in the loss of films with high embedded energy[16,17] and adds energy requirements associated with material recovery from effluent recovery-solutions and subsequent film redeposition.

Carbon-based mesoscopic perovskite solar cells (C-PSCs) present a compelling alternative to conventional PSCs, particularly for applications where cost-effectiveness, durability, and scalability are critical. This type of device consists of a triple-layer architecture of mesoporous TiO_2, a mesoporous ZrO_2

[a]SPECIFIC IKC, Materials Science and Engineering, Faculty of Science and Engineering, Swansea University, Swansea, UK

[b]School of Chemistry and Physics, University of KwaZulu-Natal, Durban, South Africa

spacer, and a carbon electrode. The full stack is screen-printed, and the perovskite is subsequently infiltrated *via* drop casting into the porous scaffold. Although power conversion efficiencies reported for C-PSCs (~20%) are lower than those of conventional devices,[18,19] they offer advantages such as compatibility with large-area, low-cost fabrication methods, and do not require costly hole-transport materials or metal electrodes.[20] Additionally, the use of 5-aminovaleric acid (AVA) helps passivate defects, suppress the escape of methylammonium iodide (MAI), and mitigate the detrimental effects of ion migration under stress conditions.[21,22] As a result, C-PSCs infiltrated with AVA-MAPI, where MAPI denotes the commonly used methylammonium lead iodide ($MAPbI_3$) composition, have been demonstrated to meet rigorous standards such as the IEC 61215:2016 stability tests.[23]

From a circularity perspective, the architecture of C-PSCs is particularly well suited to remanufacturing strategies. Because the perovskite absorber is infiltrated into the mesoporous scaffold, it remains directly accessible for post-treatment, dissolution, and reinfiltration, without requiring the removal of upper electrodes or transport layers, as is necessary in conventional device architectures.

Although research into remanufacturing methods for C-PSCs is still an emerging area of study,[24,25] their compatibility with green solvent processing and scalable manufacturing presents a compelling opportunity for sustainable EOL approaches.[20,26–28]

In this work, we explore green-solvent-based remanufacturing strategies for C-PSCs using AVA-MAPI as the perovskite absorber. Our goal was to recover the full device stack by removing the infiltrated perovskite using non-toxic solvents, thereby enabling reuse of the printed mesoporous scaffold. The solubility of lead halide salts in perovskite precursor formulations limits the range of suitable solvents. Polar aprotic solvents are typically employed because their lone pairs can coordinate to Pb^{2+} centres, promoting dissolution of PbI_2 through the formation of solvated iodoplumbate complexes. In search of greener alternatives to the typical aprotic solvents of high toxicity used for perovskite deposition, γ-valerolactone (GVL) has emerged as a promising substitute.[20,29,30] GVL is a dipolar aprotic solvent with polarity comparable to DMF, allowing efficient solvation of ionic lead-halide species with moderate coordinating strength that has led to slower and more controlled perovskite crystallisation.[29] In mesoscopic carbon-based devices, GVL has been shown to form stable, homogeneous precursor dispersions that infiltrate the porous scaffolds effectively, supporting reproducible device fabrication.[20,26] Given its established use as the precursor solvent and proven compatibility with the mesoporous stack, GVL was selected as a candidate solvent for the recovery process.

Extending the search for environmentally benign processing routes, an aqueous KOH solution was also evaluated as a water-based alternative. While PbI_2 is only sparingly soluble in water, Pb(II) compounds dissolve readily in strong acids and alkalis, forming soluble hydroxo–plumbite complexes in excess hydroxide.[31,32] The use of strong alkaline solutions such as KOH has previously been shown to remove perovskite films and recover transparent conductive oxide (TCO) substrates without damaging the underlying layers, and can even improve surface wettability.[11,33] Building on this, we explored an aqueous-based route as a greener alternative to organic solvents, offering effective dissolution of Pb species alongside simple, low-toxicity handling. Unlike sequential dissolution methods applied to planar devices, where only perovskite solubility and TCO stability are critical, the present approach required preserving the functionality of the mesoporous triple-stack scaffold, introducing an additional layer of complexity to the removal process. To this end, we tested both solvent systems, GVL (Fig. 1a) and an aqueous 1.5 M potassium hydroxide (KOH) solution (Fig. 1b), to assess whether the AVA-MAPI absorber could be effectively removed while retaining the scaffold's functionality for a second life.

Fig. 1c shows the best *J–V* curves obtained for non-aged, reinfiltrated devices. The highest power conversion efficiency (PCE) achieved using the GVL-based recovery method was 10.7%, compared to 9.1% for the KOH-based approach. For reference, the best-performing standard device from the same batch (without reinfiltration) reached a PCE of 12.1%. Electroluminescence (EL) imaging (Fig. 1e) revealed uniform perovskite emission in both the standard and GVL-rinsed devices, indicating good perovskite distribution and no apparent contact issues with the carbon counter electrode.

Although effective in other PSC architectures,[11] KOH posed challenges in the thicker, printed mesoscopic configuration, likely due to chemical interactions between its basic nature and the interfaces within the porous scaffold. While the 1.5 M KOH solution enabled second-life efficiencies of around 9%, reinfiltrated devices exhibited poor operational stability, pronounced hysteresis (Fig. S1), and limited reproducibility, particularly in aged devices, where rinsing with the KOH solution led to cloudy or visibly damaged substrates (Fig. S4 and S8) rendering many samples unsuitable for reinfiltration. Despite exhibiting uniform EL, the best-performing KOH-rinsed device showed significantly lower EL intensity compared to both the non-reinfiltrated and GVL-rinsed counterparts (Fig. 1e). This observation was consistent with steady-state photoluminescence (PL) measurements (Fig. 1d), which showed reduced emission in both reinfiltrated devices, with a more pronounced decrease in the KOH-rinsed sample. These results, together with the pronounced hysteresis and low stability, point to increased interfacial disruption between the AVA-MAPI absorber and the underlying stack in KOH-treated devices relative to those recovered using GVL.

Devices recovered using GVL demonstrated better stability (Fig. S2), and exhibited hysteresis behaviour comparable to that of standard devices (Fig. 1c and S1). To further evaluate the robustness and practical applicability of the GVL-based recovery method, we applied it to aged C-PSC devices, defined as those stored under ambient conditions for over three months. These samples exhibited initial power conversion efficiencies (PCEs) ranging from 11% to 15%, with an average PCE of 12.7%. Remanufacturing conditions were systematically varied by adjusting both the immersion time and the GVL temperature during sample immersion. Optimal rinsing conditions were identified at 85 °C, yielding average PCEs of 8.9% and 9.5% for

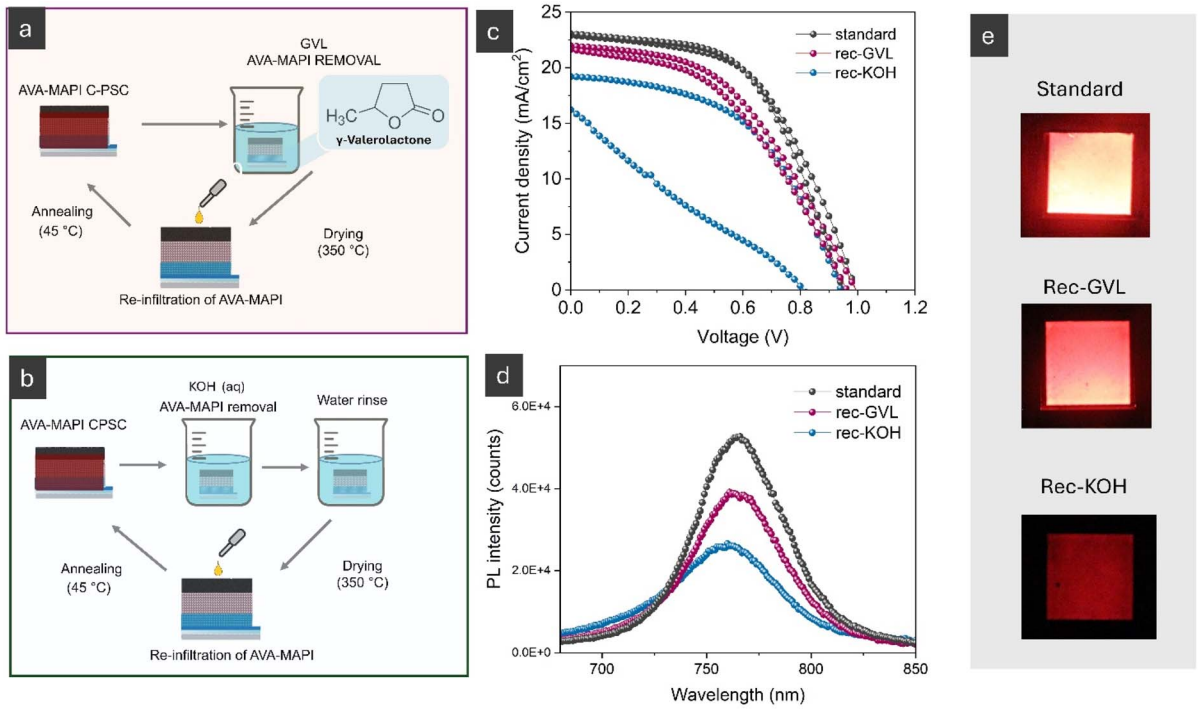

Fig. 1 Remanufacturing processes and performance of non-aged devices. Schematic illustration of the AVA-MAPI removal and re-infiltration process using (a) GVL and (b) aqueous KOH; (c) current density–voltage (*J*–*V*) curves of best-performing non-aged devices: standard, GVL-recovered, and KOH-recovered; (d) steady-state photoluminescence (PL) spectra of standard and recovered devices; (e) electroluminescence (EL) images of standard and recovered devices.

immersion times of 15 and 30 minutes, respectively (Fig. 2a). Overall, PCE recovery, defined as the second-life efficiency expressed as a percentage of the original (first-life) PCE, varied widely across tested conditions. Values ranged from 25% in the lowest-performing device to 89% in the best case, where a second-life efficiency of 12.4% was achieved from a device with a first-life PCE of 13.9% (Fig. 2b).

XRD patterns of GVL-rinsed scaffolds (Fig. S7) show no PbI_2 reflections for either short (3 min, 25 °C) or extended (20 min, 85 °C) treatments. The lack of detectable Pb-containing phases suggests that differences in post-processing conditions likely arise from trace-level residues below the XRD detection threshold rather than bulk PbI_2. The integrity of the carbon counter electrode was likely a key factor contributing to the high variability in device performance after recovery. While moderate damage to the carbon film in aged devices did not significantly impact first-life efficiency, surface imperfections became critical during remanufacturing. These defects hindered uniform perovskite removal throughout the stack, ultimately leading to samples unfit for reinfiltration (Fig. S5).

PL and TRPL measurements provide insight into the limitations causing remanufactured devices to exhibit lower PCEs than first-life devices. These measurements were performed on complete devices, with excitation incident through the glass substrate, thereby illuminating the TiO_2 mesoporous scaffold side of the stack. Excitation wavelengths of 450 nm (PL) and 405 nm (TRPL) were used, which, given the perovskite's absorption coefficient ($\sim 10^5$ cm^{-1}), correspond to a penetration depth of less than 1 μm.[34] As a result, the data primarily reflect the perovskite within the TiO_2 mesoporous scaffold. The results show variable PL intensities (Fig. 2c), sometimes exceeding those of pristine devices, as well as peak shifts and consistently shorter TRPL, with τ_2 dropping from over 30 ns in first life devices to 22 ns and even as low as 5 ns (Fig. 2d).

A PL blue-shift of approximately 5 nm was observed for the KOH-treated non-aged sample relative to the standard and GVL-recovered samples, both of which show a PL emission peak at approximately 765 nm (Fig. 1d). Although this initial evaluation was carried out on non-aged recovered devices and appears to show a solvent-dependent effect, a wide variation in peak position was also observed in aged devices recovered using GVL. PL blue-shift and apparent bandgap widening have been widely linked to differences in perovskite crystallisation and microstructure: smaller grain size, increased disorder, and lattice strain, arising from confinement within mesoporous scaffolds or from structural variations between surface and edge regions in MAPI single crystals, can all shift the emission to higher energies.[35–38] Alternatively, partial degradation or PbI_2 formation has also been shown to produce blue-shifted and broadened PL spectra.[39] The variability observed here likely reflects local differences in perovskite crystallisation, strain, and degradation within the mesoporous stack, influenced by both solvent-specific effects on the infiltration environment and variations in the structural integrity of individual stacks. These factors together help explain the observed spread in device performance.

Thermal and solvent stress during GVL rinsing and subsequent drying at 350 °C, along with the presence of residual

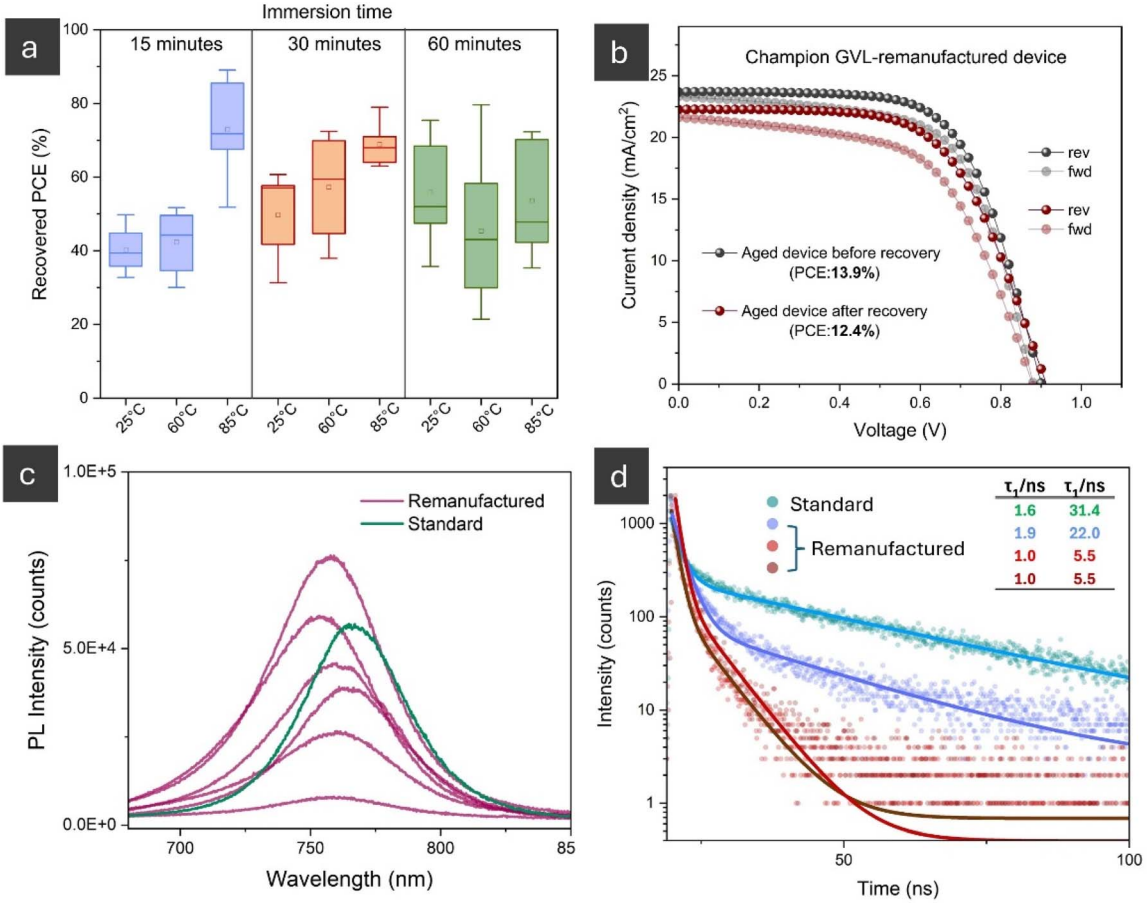

Fig. 2 Remanufacturing of aged carbon-based perovskite solar cells *via* GVL rinsing. (a) Recovered power conversion efficiency (PCE), expressed as a percentage of the original efficiency, for devices remanufactured by immersion in γ-valerolactone (GVL) at different temperatures and durations. (b) Current density–voltage (*J*–*V*) characteristics of the best-performing remanufactured device, before and after GVL recovery. (c) Steady-state photoluminescence (PL) spectra and (d) time-resolved PL (TRPL) decay curves comparing standard (fresh) and remanufactured devices.

perovskite, may induce chemical or morphological changes at the perovskite interfaces on samples subject to recovery and reinfiltration. These alterations can impair infiltration quality, evidenced by reduced PL intensity, or disrupt charge collection at the interfaces, as suggested by cases where higher PL intensity is accompanied by shorter carrier lifetimes. Together, the reduced performance of remanufactured devices, along with PL and TRPL data, points to multiple mechanisms contributing to performance loss, primarily related to disruption of the printed mesoporous scaffold, which may hinder perovskite infiltration and lead to interfacial disruption.[40]

While the recovered performance does not match that of pristine devices, these results provide compelling evidence of the structural resilience of the full mesoporous stack. This is a key finding from a circular design perspective: the ability to rinse and reuse the scaffold without re-depositing each layer represents a substantial reduction in energy and material input, a trade-off that could be acceptable if long-term stability can be achieved.[41] Conventional scaffold fabrication is an energy-intensive process, typically requiring sintering at 400–550 °C for each oxide layer. The mesoporous transport layer represents a major energy input in PSC manufacturing, with studies indicating that substrate patterning, spray pyrolysis of TiO_2, and the deposition and sintering of the mesoporous layer can jointly account for up to 74% of the total energy demand in conventional mesoscopic PSCs.[16] In carbon-based architectures, this share is even higher due to the absence of gold evaporation and the inclusion of additional printed layers requiring multiple sintering steps.[16,17] These findings highlight the substantial energy investment embodied in the mesoporous scaffold and underscore the importance of remanufacturing strategies that enable its reuse.

Conclusions

In summary, carbon-based perovskite solar cells (C-PSCs) can be effectively remanufactured using sustainable, non-destructive methods that preserve the original device architecture and enable a functional second life for the device. While the KOH-based method enabled partial recovery of device performance, achieving a maximum reinfiltrated efficiency of 9.1% for non-aged devices, it was limited by poor stability, low

reproducibility, and structural disruption in aged scaffolds. Future efforts aimed at mitigating scaffold disruptions during recovery with KOH solutions could make this water-based approach an attractive and scalable alternative for sustainable device remanufacturing. The GVL-based rinsing and reinfiltration strategy proved successful for both non-aged and ambient-aged devices, maintaining functional interfaces and restoring up to 89% of the original (first-life) efficiency. This approach offers a practical route to extending the operational lifetime of devices without requiring mesoporous stack redeposition or high-temperature reprocessing.

Future work focused on optimising rinsing conditions, enhancing interface passivation, and preserving the structural integrity of the carbon layer could further improve remanufacturing outcomes, potentially achieving efficiencies comparable to those of pristine devices. By enabling the reuse of critical device components and minimizing the need for energy- and resource-intensive processing, this strategy represents a key step toward more circular and sustainable perovskite photovoltaic technologies.

Conflicts of interest

There are no conflicts to declare.

Data availability

The data supporting this article have been included as part of the supplementary information (SI). Supplementary information: details of materials, experimental procedures, characterisation data, and additional documentation. See DOI: https://doi.org/10.1039/d5su00707k.

Acknowledgements

The authors are grateful for funding from UKRI and the EU Horizon Europe Framework Programme (101122277) to support the APOLLO project. This work was made possible by support from the Engineering and Physical Sciences Research Council (EP/S001336/1 and EP/X025217/1) and through the funding of the SPECIFIC Innovation and Knowledge Centre by EPSRC (EP/N020863/1), Innovate UK [920036], and the European Regional Development Fund [c80892] through the Welsh Government. MLD and TMW are also grateful for funding of the TEA@-SUNRISE project, funded with UK aid from the UK government *via* the Transforming Energy Access platform, and to funding from the UK Government's Ayrton Challenge through the International Science Partnerships Fund (ISPF) as part of the REACH-PSM project.

Notes and references

1 IRENA, *World Energy Transitions Outlook 2023: 1.5°C Pathway*, International Renewable Energy Agency, Abu Dhabi, 2023, vol. **1**.
2 J. C. Goldschmidt, L. Wagner, R. Pietzcker and L. Friedrich, *Energy Environ. Sci.*, 2021, **14**, 5147–5160.
3 R. G. Charles, A. Doolin, R. García-Rodríguez, K. V. Villalobos and M. L. Davies, *Energy Environ. Sci.*, 2023, **16**, 3711–3733.
4 A. Wade, G. Heath, S. Weckend, K. Wambach, P. Sinha, Z. Jia, K. Komoto and K. Sander, *IRENA and IEA PVPS, End-Of-Life Management: Solar Photovoltaic Panels*, 2016.
5 G. Heath, T. Silverman, M. Kempe, M. Deceglie, D. Ravikumar, T. Remo, H. Cui, P. Sinha, C. Libby, S. Shaw, K. Komoto, K. Wambach, E. Butler, T. Barnes and A. Wade, *Nat. Energy*, 2020, **5**, 502–510.
6 V. Fthenakis and E. Leccisi, *Prog. Photovoltaics Res. Appl*, 2021, **29**, 1068–1077.
7 J. H. Wong, M. Royapoor and C. W. Chan, *Renew. Sustain. Energy Rev.*, 2016, **58**, 608–618.
8 A. Babayigit, A. Ethirajan, M. Muller and B. Conings, *Nat. Mater.*, 2016, **15**, 247–251.
9 G. Ding, Y. Zheng, X. Xiao, H. Cheng, G. Zhang, Y. Shi and Y. Shao, *J. Mater. Chem. A*, 2022, **10**, 8159–8171.
10 *NREL Best Research-Cell Efficiency Chart*, https://www.nrel.gov/pv/cell-efficiency/, accessed July, 2025.
11 B. Augustine, K. Remes, G. S. Lorite, J. Varghese and T. Fabritius, *Sol. Energy Mater. Sol. Cells*, 2019, **194**, 74–82.
12 A. Binek, M. L. Petrus, N. Huber, H. Bristow, Y. Hu, T. Bein and P. Docampo, *ACS Appl. Mater. Interfaces*, 2016, **8**, 12881–12886.
13 M. S. Chowdhury, K. S. Rahman, V. Selvanathan, A. K. M. Hasan, M. S. Jamal, N. A. Samsudin, M. Akhtaruzzaman, N. Amin and K. Techato, *RSC Adv.*, 2021, **11**, 14534–14541.
14 K. Wang, T. Ye, X. Huang, Y. Hou, J. Yoon, D. Yang, X. Hu, X. Jiang, C. Wu, G. Zhou and S. Priya, *Matter*, 2021, **4**, 2522–2541.
15 X. Xiao, N. Xu, X. Tian, T. Zhang, B. Wang, X. Wang, Y. Xian, C. Lu, X. Ou, Y. Yan, L. Sun, F. You and F. Gao, *Nature*, 2025, **638**, 670–675.
16 A. L. Carneiro, A. A. Martins, V. C. M. Duarte, T. M. Mata and L. Andrade, *Energy Rep.*, 2022, **8**, 475–481.
17 T. Ibn-Mohammed, S. C. L. Koh, I. M. Reaney, A. Acquaye, G. Schileo, K. B. Mustapha and R. Greenough, *Renew. Sustain. Energy Rev.*, 2017, **80**, 1321–1344.
18 S. Liu, D. Zhang, Y. Sheng, W. Zhang, Z. Qin, M. Qin, S. Li, Y. Wang, C. Gao, Q. Wang, Y. Ming, C. Liu, K. Yang, Q. Huang, J. Qi, Q. Gao, K. Chen, Y. Hu, Y. Rong, X. Lu, A. Mei and H. Han, *Fundam. Res.*, 2022, **2**, 276–283.
19 Y. Zhang, Y. Chen, Y. Liu, Y. Cai, Y. Liu, C. Wu, J. Wang, Z. Zhang, D. Wang and J. Zhang, *Small*, 2025, **21**, 2410856.
20 C. Worsley, D. Raptis, S. Meroni, A. Doolin, R. Garcia-Rodriguez, M. Davies and T. Watson, *Energy Technol.*, 2021, **9**, 2100312.
21 A. Mei, X. Li, L. Liu, Z. Ku, T. Liu, Y. Rong, M. Xu, M. Hu, J. Chen, Y. Yang, M. Grätzel and H. Han, *Science*, 2014, **345**, 295–298.
22 E. V. Péan, C. S. De Castro, S. Dimitrov, F. De Rossi, S. Meroni, J. Baker, T. Watson and M. L. Davies, *Adv. Funct. Mater.*, 2020, **30**, 1909839.
23 A. Mei, Y. Sheng, Y. Ming, Y. Hu, Y. Rong, W. Zhang, S. Luo, G. Na, C. Tian, X. Hou, Y. Xiong, Z. Zhang, S. Liu, S. Uchida,

T.-W. Kim, Y. Yuan, L. Zhang, Y. Zhou and H. Han, *Joule*, 2020, **4**, 2646–2660.
24 L. Hong, Y. Hu, A. Mei, Y. Sheng, P. Jiang, C. Tian, Y. Rong and H. Han, *Adv. Funct. Mater.*, 2017, **27**, 1703060.
25 D. Bogachuk, P. van der Windt, L. Wagner, D. Martineau, S. Narbey, A. Verma, J. Lim, S. Zouhair, M. Kohlstädt, A. Hinsch and S. D. Stranks, *ACS Sustainable Resour. Manage.*, 2024, **1**, 417–426.
26 C. Worsley, D. Raptis, S. Meroni, R. Patidar, A. Pockett, T. Dunlop, S. J. Potts, R. Bolton, C. M. E. Charbonneau, M. Carnie, E. Jewell and T. Watson, *Mater. Adv.*, 2022, **3**, 1125–1138.
27 R. Vidal, J.-A. Alberola-Borràs, S. N. Habisreutinger, J.-L. Gimeno-Molina, D. T. Moore, T. H. Schloemer, I. Mora-Seró, J. J. Berry and J. M. Luther, *Nat. Sustain.*, 2021, **4**, 277–285.
28 G. Rodriguez-Garcia, E. Aydin, S. De Wolf, B. Carlson, J. Kellar and I. Celik, *ACS Sustainable Chem. Eng.*, 2021, **9**, 15239–15248.
29 F. Kerkel, M. Markiewicz, S. Stolte, E. Müller and W. Kunz, *Green Chem.*, 2021, **23**, 2962–2976.
30 J. Bae, J. Cha, M. Kim and J. Han, *Green Chem.*, 2025, **27**, 10598–10611.
31 W. N. Perera, G. Hefter and P. M. Sipos, *Inorg. Chem.*, 2001, **40**, 3974–3978.
32 P. Patnaik, *Handbook of Inorganic Chemicals*, McGraw-Hill, New York, NY, 2003.
33 M. V. Gallegos, L. Gil-Escrig, K. P. S. Zanoni, H. J. Bolink and L. C. Damonte, *Sol. Energy Mater. Sol. Cells*, 2024, **277**, 113117.
34 N.-G. Park, *Mater. Today*, 2015, **18**, 65–72.
35 W. Nie, H. Tsai, R. Asadpour, J.-C. Blancon, A. J. Neukirch, G. Gupta, J. J. Crochet, M. Chhowalla, S. Tretiak, M. A. Alam, H.-L. Wang and A. D. Mohite, *Science*, 2015, **347**, 522–525.
36 Z. Zhang, M. Wang, L. Ren and K. Jin, *Sci. Rep.*, 2017, **7**, 1918.
37 G. Grancini, V. D'Innocenzo, E. R. Dohner, N. Martino, A. R. Srimath Kandada, E. Mosconi, F. De Angelis, H. I. Karunadasa, E. T. Hoke and A. Petrozza, *Chem. Sci.*, 2015, **6**, 7305–7310.
38 J. J. Choi, X. Yang, Z. M. Norman, S. J. L. Billinge and J. S. Owen, *Nano Lett.*, 2014, **14**, 127–133.
39 E. V. Péan, C. S. De Castro and M. L. Davies, *Mater. Lett.*, 2019, **243**, 191–194.
40 E. V. Péan, S. Dimitrov, C. S. De Castro and M. L. Davies, *Phys. Chem. Chem. Phys.*, 2020, **22**, 28345–28358.
41 J. Bilbao, G. Heath, A. Norgren, M. Monteiro Lunardi, A. Carpenter and R. Corkish, PV Module Design for Recycling, *IEA-PVPS Report T12-23:2021*, International Energy Agency Photovoltaic Power Systems Programme, 2021.